



HAL
open science

Sound and Vision: Visualization of music with a soap film, and the physics behind it

C Gaulon, C Derec, T Combriat, P Marmottant, F Elias

► **To cite this version:**

C Gaulon, C Derec, T Combriat, P Marmottant, F Elias. Sound and Vision: Visualization of music with a soap film, and the physics behind it. 2017. hal-01487166

HAL Id: hal-01487166

<https://hal.science/hal-01487166>

Preprint submitted on 11 Mar 2017

HAL is a multi-disciplinary open access archive for the deposit and dissemination of scientific research documents, whether they are published or not. The documents may come from teaching and research institutions in France or abroad, or from public or private research centers.

L'archive ouverte pluridisciplinaire **HAL**, est destinée au dépôt et à la diffusion de documents scientifiques de niveau recherche, publiés ou non, émanant des établissements d'enseignement et de recherche français ou étrangers, des laboratoires publics ou privés.

Sound and Vision: Visualization of music with a soap film, and the physics behind it

C. Gaulon¹, C. Derec¹, T. Combriat², P. Marmottant² and F. Elias^{1,3}

¹ Laboratoire Matière et Systèmes Complexes UMR 7057, Université Paris Diderot, Sorbonne Paris Cité, CNRS, F-75205 Paris, France

² Laboratoire Interdisciplinaire de Physique LIPhy, Université Grenoble Alpes and CNRS UMR 5588

³ Sorbonne Universités, UPMC Univ Paris 06, 4 place Jussieu, 75252 PARIS cedex 05, France

florence.elias@univ-paris-diderot.fr

Abstract

A vertical soap film, freely suspended at the end of a tube, is vibrated by a sound wave that propagates in the tube. If the sound wave is a piece of music, the soap film comes alive: colours, due to the soap film iridescences, swirl, split and merge at the rate of the music (see the snapshots on figure 1 below). In this article, we analyse the rich physics behind those fascinating dynamical patterns: it combines the acoustic propagation in a tube, the light interferences, and the static and dynamic properties of soap films. The interaction between the acoustic wave and the liquid membrane results in capillary waves on the soap film, as well as non-linear effects leading to a non-oscillatory flow of liquid in the plane of the film, which induces several spectacular effects: vortices generation, diphasic dynamical patterns inside the film, and swelling of the soap film under certain conditions. Each of these effects is associated with a characteristic time scale, which interacts with the characteristic time of the music play. This article shows the richness of those characteristic times that lead to dynamical patterns. Through its artistic interest, the experiments presented in this article provide a tool for popularizing and demonstrating science in classroom or broader audience.

1 Introduction

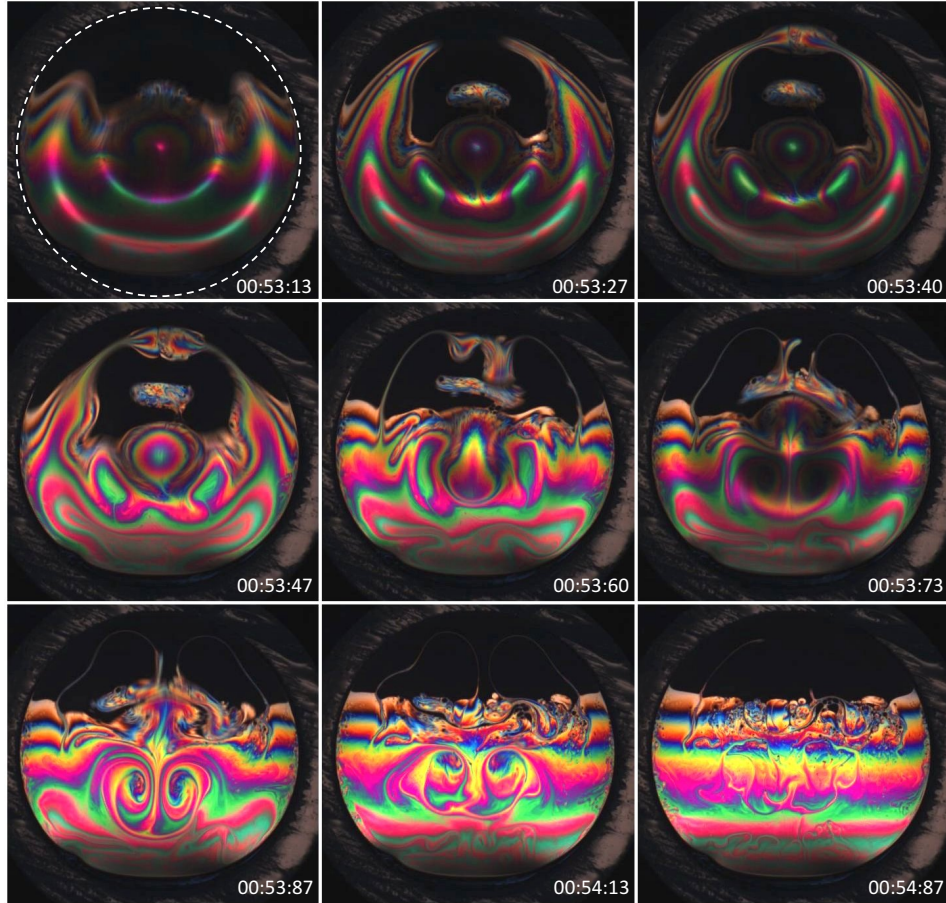


Figure 1: Snapshots of the observed dynamics in a freely suspended vertical soap film submitted to an acoustic wave and illuminated by a white light (colours onlie). The dashed white circle on the first picture shows the internal border of the tube (of diameter $D = 26$ mm) delimiting the soap film. Piece of music: *Lucilla*, from the album ‘Aeroplanando’, by Choro de Rua (2013) (see the video at the following link: <https://youtu.be/ch1m9vrgAzM>). The time of each snapshot is indicated in the format minute:seconds:hundredths of second, starting from the beginning of the piece.

For many centuries, both scientists and artists have been searching for connec-

tions between sound and vision, in other words between what we hear and what we see. Historically, these connections were first searched between music and colour. Aristotle, in his *De sensu et sensibilibus*, considered seven colours distributed from Black to White [1]. This was based on the analogy with the Pythagorean intervals in music, that define seven notes: Aristotle transferred the consonances of tonal intervals to colours. Inspired by the work of the ancient Greeks, Newton represented the decomposition of white light through a prism with seven colours. In his *Opticks*, in 1704, this was illustrated with the so-called Newton’s circle, that shows the colours correlated with musical notes A to G [2], as represented in Fig. 2(a). The spectral colours are divided by the musical notes, the note D being arbitrarily placed between the red and the violet: the circle thus complete a full octave. In 1893, the british painter Alexander Wallace Rimington invented an instrument, also based on the correlation between colour and music, the Colour Organ [3]. A coloured light was projected when the associated note was played. In 2015, the

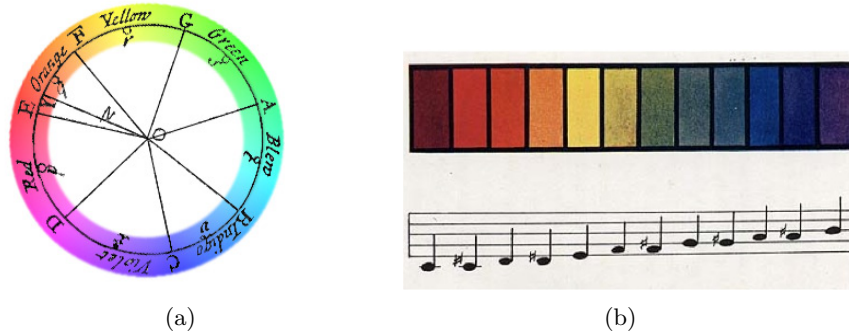


Figure 2: Two different ways of associating colours to musical notes (colours online). (a) Newton’s circle. Colours from red to violet are divided by notes, starting arbitrarily at D with purple colour (from [2]). (b) Rimington’s chromatic scale in Music and Colour, starting arbitrarily at C with dark red colour (from [3]).

National Gallery in London presented the exhibition “Soundscapes”, judiciously subtitled “Hear the painting. See the sound” [4]. Some musicians and sound artists were asked to choose a painting from the museum collection, and compose a new piece of music in response, in order to create an immersive and original experience. Recently, the musician Nigel Stanford published a music-clip where the music is visualized using physics experiments [5], including Faraday instabilities, the use of ferrofluids, and the sand patterns of Chladni plates.

In this article, we propose a new way to visualize music, using a soap film. Similarly to Stanford’s performances, the genuine connection between sound and vision comes from the fact that what we see (the transverse vibration of the soap film, the vortices) is generated by what we hear. As we will describe later, many physical phenomena come into play and combine together, creating aesthetic effects.

On top of their artistic interest, soap films are commonly used for demonstrating science in classroom or broader audience [6–9]. Soap films and bubbles consist in a thin liquid film, which are stabilized by surfactant molecules; they tend to decrease their interfacial energy by minimizing the area of their interfaces. Hence, the science of soap films is by essence at a crossroads between physics, mathematics and chemistry. Soap films and bubbles also provide analogy to other physical systems such as atmospheric phenomena (stratification and turbulence [10, 11]) and mathematics (catastroph theory and minimisation problems [8, 9]).

Vibrating soap films and the associated patterns have fascinated physicists for long times. In 1877, E. B. Tylor reported about the “singular clearness and beauty” of the patterns formed on a soap film “by talking, singing and playing a cornet in its neighborhood” [12]. One year later, S. Taylor published drawings illustrating the symmetry of the patterns obtained when a horizontal soap film was submitted to a monochromatic acoustic wave [13]. Many studies have tempted to rationalize those phenomena [10, 14–18]. The underlying physics resides in the hydrodynamics of the liquid and the surrounding air, and the way those flows are coupled at the liquid interfaces of the thin film.

In a previous article, soap films have been used to visualize a monochromatic standing sound wave in a tube [19]. This visualization was based on the interaction between the soap films placed inside the tube, the acoustic wave and the optical wave. In the present article, only one film is formed at the end of a tube. The dynamics of the soap film is observed in response to a non-continuous acoustic forcing: a music play, applied at the other end of the tube. We analyse the physical phenomena involved in this rich and spectacular dynamics. This makes of this experiment an appropriate tool to teach the physics of light interference, acoustic resonance as well as the vibrations of membranes and the physics of thin liquid films.

The article is organized as follows. The set-up is described in section 2 and some background is exposed in section 3. The film, placed at the end of a tube submitted to an acoustic wave, vibrates like a fluid membrane. The vibration amplitude is maximum at the *resonance* frequencies of the tube (section 3.1). The colours are due to *interferences* of the light reflected by both air-liquid interfaces of the film (section 3.2), whose stability is due to the presence of *surfactant molecules*. The colour gradients reflect thicknesses gradients of the soap film, which slowly evolve due to the *gravity induced drainage* of the liquid within the film when the soap film is quiet (section 3.3). The dynamics of the soap film due to the acoustic forcing is then described in section 4, and illustrated in Fig. 1. The different physical ingredients are described one by one in this section. The acoustic forcing generates transverse *capillary standing waves* on the liquid membrane, which are revealed by the observation of bright concentric rings on the film (section 4.1). At large enough forcing amplitude, local thickness variation appear within the film, following the spatial periodicity of the capillary wave: this thickness modulation is known as a *self-adaptation* mechanism (section 4.2). At larger forcing amplitude, counter-rotative vortices appear within the soap film (section 4.3). The tangential flows inside the film eventually advect regions of different thicknesses, which do not mix

and form two-dimensional drops in the film (section 4.4). A large recirculation of liquid inside the film has also been observed, which can lead to the *swelling* of a previously drained film (section 4.5). As a conclusion, we point out in section 5 the key elements to perform this Sound and Vision experiment in an aesthetic way.

2 Experimental set-up

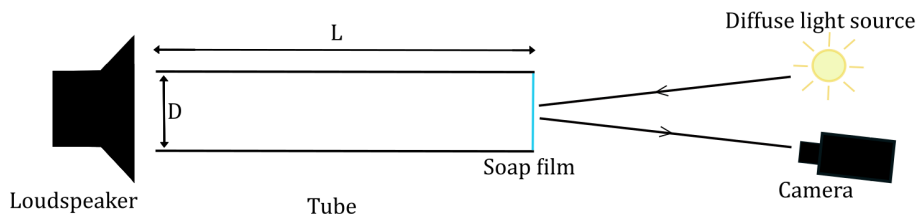


Figure 3: Sketch of the experimental set-up. The diffusive light source is obtained using a table lamp and a diffusive screen made of tracing paper between the lamp and the soap film.

An acoustic wave is generated by a loudspeaker connected to a frequency generator. The loudspeaker is placed at one end of a horizontal cylindrical plexiglas tube, of length $L = 35.5$ cm, and internal diameter $D = 26$ mm. The tube is filled with air at ambient temperature and atmospheric pressure. At the other end of the tube, a vertical soap film is formed by placing the tube vertically and dipping its end into a soap solution, and by placing back the tube in the horizontal position. The soap solution is made of distilled water, 10% of commercial washing liquid (Fairy[®] liquid, Dreft[®] or Dawn[®] – which are different brands of the same product by Procter and Gamble) and 10% of glycerol (the percentages are indicated in volume). For the visualization of the soap film we use a diffuse light source, and a camera that receives the light reflected by the film (Fig. 3). The videos are recorded at a frame rate of approximately 13 frames per second. A video presenting the setup is visible at the following link: <https://youtu.be/wMFrWZpVMM>.

In the next sections, we will describe each one of these elements.

3 Scientific background

In this section, we present separately the different physical ingredients of the experiment: the sound wave propagation in the tube, the visualization of the soap film, and some considerations about the physics of the soap film.

3.1 Acoustic resonances in a tube

In this subsection, we consider an open tube, without soap film. The incident propagative wave is reflected at the end of the tube. Both incident and reflected waves add up, leading to a standing wave in the tube for some specific frequencies: the resonance frequencies. At these frequencies, the acoustic pressure P in the tube, which is a small deviation around the atmospheric pressure, is maximum. The experimental resonance frequencies can be measured using a microphone at the other end of the tube. The microphone is calibrated using a sound level meter, giving an information in Decibel, which can be easily converted in a pressure in Pascal.¹ The measurements are presented on Fig. 4(a), where the forcing consists in a frequency sweep (total duration = 40 s) and the acoustic pressure is measured during the sweep at the end of the tube (blue curve): the resonances, corresponding to the maximal amplitude, are clearly visible. For comparison, we have reported on the same plot the acoustic pressure measured at the same position when the tube is removed (black curve). Not only the resonances disappear in this last case, but also the acoustic amplitude is much lower than at the exit of the tube even in the minimums of the blue curve, showing that the tube also acts as a waveguide.

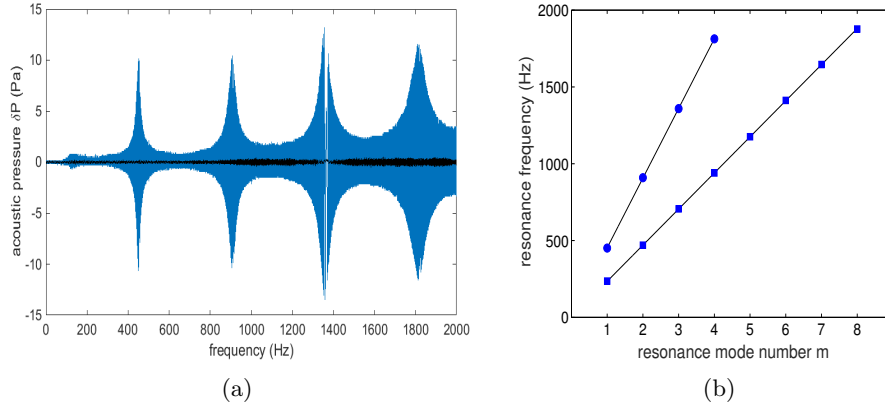


Figure 4: (a) Acoustic pressure P versus the frequency f of the forcing sound wave, measured at the end of the tube (blue curve) and at the same position without the tube (black curve). b) Resonance frequencies versus the mode number m , for two different tube lengths: $L = 35.5$ cm (circles) and $L = 70$ cm (squares), of same diameter $D = 26$ mm. The black lines correspond to the theoretical expression of the resonance frequencies, given by equation (3), and adjusting the end correction C to the best fit.

¹The relation between the sound pressure level L_P (dB) and the pressure P (Pa) is $L_P = 20 \log_{10}(P/P_{ref})$ where $P_{ref} = 20 \mu\text{Pa}$ is the reference pressure corresponding to 0 dB.

In Fig. 4(b), the experimental resonance frequencies f_m are identified for two tubes of different lengths and of same diameter, and plotted versus the resonant mode number m (corresponding to the number of antinodes inside the tube). We see that the longer tube has the lower first resonance frequency, and also has, in the same interval of frequencies, more resonances.

These experimental results can be modelled as follows. The resonance frequencies depend on the boundary conditions: in our case, at one end the loudspeaker is a vibrating membrane, leading to a maximum (an anti-node) of acoustic displacement and so to a node of acoustic pressure. At the other end, the open end of the tube is a node of acoustic pressure and a maximum of acoustic displacement (that is why this configuration is often called a two open-ends tube). Note that this two open-ends tube configuration will still be valid with the soap film. These boundary conditions force only a discrete number of wavelengths λ_m for the standing wave inside the tube. These wavelengths are given by the relation:

$$\lambda_m = \frac{2L}{m}, \quad (1)$$

where m is called the resonance mode number. The resonance frequencies can be deduced, since $\lambda = v/f$, with v the sound velocity in air:

$$f_m = m \frac{v}{2L}. \quad (2)$$

A more accurate expression of the resonance frequencies can be written by taking into account the diameter of the tube. The tube is “acoustically seen” longer than it is in reality, and a standing wave inside has a wavelength $\lambda_m = 2(L + 2C)/m$ [20]. C represents the end correction (on each end), and is proportional to the diameter. The resonance frequencies, previously given by eq. (2), are written with this improved model as follows:

$$f_m = m \frac{v}{2(L + 2C)}. \quad (3)$$

Eq. (3) is shown as black lines in Fig. 4(b), where C has been adjusted, for each tube, to the best fit (taking $v = 343$ m/s). We obtain $C = (0.47 \pm 0.02) D$ for $L = 35.5$ cm and $C = (0.42 \pm 0.02) D$ for $L = 70$ cm: both cases are consistent with values found in the literature (see for example the theoretical model [21] where $C \simeq 0.42D$).

3.2 The colours of a soap film: light interferences

At one end of the tube, a vertical soap film is freely suspended at the internal border of the tube. The film is illuminated with a white light source, and observed under the incidence angle using a video camera (see Fig. 3). A colourful pattern is visible on the soap film even when no acoustic forcing is imposed, as it can be

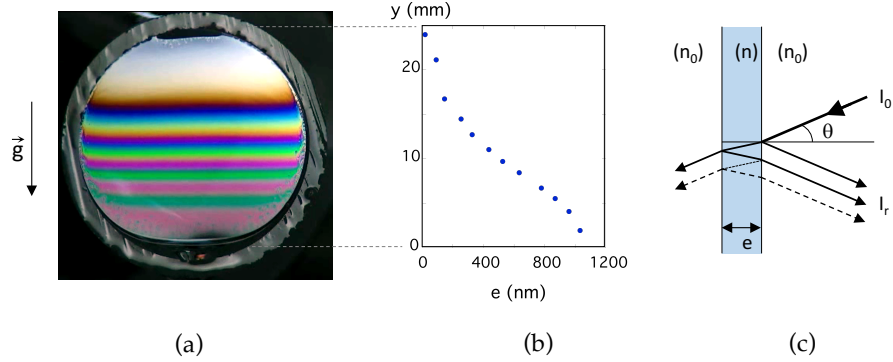


Figure 5: (a) Photograph of a soap film without any acoustic forcing (colours online): the soap film is vertical and displays a variation of colours, corresponding to a thickness gradient due to the gravitationally driven drainage. (b) Thickness of the film along the vertical direction y . The measurements are based on the colour of the film at height y (see text). (c) Interference caused by light travelling along different paths through a film. I_0 is the incident light intensity and I_r is the intensity of the light reflected by the soap film. n and n_0 are respectively the optical index of the soap solution and of air.

seen on Fig. 5(a): horizontal iridescent fringes are observed, which slowly move downwards in time.

Those colours have the same origin as the irisations observed in an oil slick on the surface of water: they result from the interferences of the light reflected by both liquid-air interfaces, when the film thickness is of the order of the wavelength of visible light. Using a monochromatic illumination of wavelength λ_ℓ , the reflected light intensity I_r is given by:

$$I_r^{\lambda_\ell}(e) = 2RI_0 \left[1 - \cos \left(\frac{2\pi\delta(e)}{\lambda_\ell} \right) \right] \quad \text{with} \quad \delta(e) = 2e\sqrt{n^2 - \sin^2 \theta} \quad (4)$$

where R is the reflection coefficient of light at the air-liquid interface, δ is the optical path difference, n the optical index of the soap solution and θ is the incident angle as sketched in Fig. 5(c) [8].² Eq. (4) shows that when the soap film thickness e varies, the light intensity oscillates between zero and a maximum value, which correspond respectively to destructive and constructive interferences. When e varies from a

²The negative sign before the cosine in equation (4) comes from the π phase-shift during the second reflection, from a medium of index n to a medium of index $n_0 < n$. The multiple reflection of light, represented by a dashed line in Fig. 5(c), can be neglected because of the low value of $R \simeq 2.5$ %.

quantity Δe such as $\Delta\delta = \lambda_\ell$, then $I_r^{\lambda_\ell}(e + \Delta e) = I_r^{\lambda_\ell}(e)$: from one dark fringe to the next one, the optical path difference has varied from one wavelength.

The white light illumination contains all the wavelengths in the visible spectrum between 400 nm and 800 nm. The reflected intensity corresponding to each wavelength add up:

$$I_r(e) = \int I_r^{\lambda_\ell}(e) g(\lambda_\ell) d\lambda_\ell \quad (5)$$

where $g(\lambda_\ell)$ describes the characteristic spectrum distribution of the light. If $I_r^{\lambda_\ell} \neq 0$ for every wavelength, the intensities add up and the resulting colour is white. In contrast, when e reaches a value such as the interference is destructive for one particular wavelength λ_ℓ , the observed colour is the complementary colour on the visible spectrum. Hence, the soap film appears white for $\delta \simeq 400$ nm, and then successively yellow, pink, blue, etc., when δ increases, which correspond respectively to a destructive interference for $\lambda_\ell \simeq 450$ nm (blue), $\lambda_\ell \simeq 530$ nm (green), $\lambda_\ell \simeq 570$ nm (yellow), etc. When the thickness increases, the contrast decreases and the film becomes light pink and light green. When the optical path becomes larger than the coherence length of the light source (typically $1 \mu\text{m}$ for an incandescent light bulb), the iridescent pattern completely loses contrast and becomes uniformly white. On the opposite, when δ is smaller than the visible wavelength (typically when $\delta < 200$ nm), the interferences are destructive and the intensity of the reflected light tends to zero (see Eq. 4). In absence of any other source of light, the soap films thus appears black. The coloured interference fringes described in this section are referred to as Newton's shades, since Newton was the first one to describe those shades in his *Opticks* [2].

The thickness of a soap film can therefore be determined using charts on the optical path that have been established using a white light illumination [8, 22]. However, since the colors travel periodically through the entire visible spectrum when the thickness increases, the chart can be used only if the soap film thickness varies continuously and monotonously, starting from the black film, visible on the image. The soap film profile in Fig. 5 has been measured according to this method (with the area of black film visible at the top of the film). The soap film thickness can also be measured using a spectrometer, which splits the white light into separate wavelengths λ_ℓ using an optical grating; $I_r^{\lambda_\ell}(e)$ is then measured as a function of λ_ℓ and the value of e corresponds to the best fit of the data using Eq. (4) [23].

3.3 Stability and dynamical properties of a soap film

Contrary to the case of a film made of pure water, a soap film can be stable in time. This stability is due to the surfactant molecules, also called amphiphilic molecules. Surfactant molecules are composed of two antagonist parts linked by a covalent bond: a hydrophilic end and another end less soluble in water, usually referred to as "hydrophobic". The hydrophobic part, generally a chain of Carbon and Hydrogen, is called the tail; the hydrophilic part, generally charged or dipolar, is smaller and referred to as the head, as sketched on Fig. 6(a). The surfactant molecules thus tend to adsorb at the interface of water (or any ionic liquid), with

their hydrophilic head plunging in the liquid and their hydrophobic tail pointing in the air, as sketched on Fig. 6(b). The surfactant molecules stabilize the soap film via two main effects.

3.3.1 Long-time stabilisation: equilibrium thickness

First of all, the surfactant coverage provides a repulsive interaction between the air-liquid interfaces, which counterbalances the van der Waals attraction. The repulsion is either electrostatic if the surfactant is ionic, or steric in the case of a non-ionic surfactant.³ The competition between attractive and repulsive interactions results in an equilibrium thickness, of the order of a few tens of nanometers in the case of an electrostatic repulsion and of a few nanometers in the case of a steric repulsion. Equilibrium soap films are referred to as common black film in the first case, and Newton black film in the second case. Both soap films indeed appear black when illuminated as described in the previous section, because the optical path is smaller than the wavelength of the visible light.

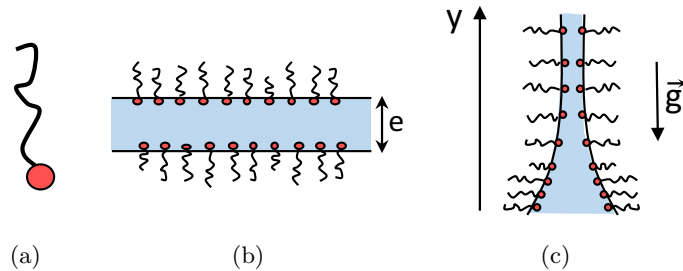


Figure 6: (a) Sketch of a surfactant molecule, made of a hydrophilic head and a hydrophobic tail. The total length of the molecule is of the order of a nanometer. (b) Sketch of the cross-section of a soap film, consisting of a thin layer of liquid bordered with two monolayers of surfactant molecules adsorbed at the liquid-air interfaces. (c) Sketch of a cross-section of a vertical soap film: the thickness gradient is accompanied with a gradient of surface concentration of the surfactant molecules at the interfaces. Panels (b) and (c) are not drawn to scale.

3.3.2 Short-time: hydrostatic quasi-equilibrium and elasticity

Soap films do not immediately reach their equilibrium thickness. A few seconds after their formation, vertical soap films display a pattern of parallel horizontal col-

³The thermodynamics of such interacting interfaces is well described in the case of an electrostatic repulsion by the so-called DLVO theory (which also describes the colloidal stability of sub-micrometric particles in a liquid) [24].

orful fringes as shown on Fig. 5(a), whereas a liquid film without surfactant would spontaneously break. This pattern reveals a stratification of the thickness of the soap film, suggesting that a hydrostatic equilibrium has been reached, as described in many publications and summarized by Couder *et.al.* [10]. The adsorption of tensioactive molecules modifies the surface tension of the air-liquid interface: the larger the surface concentration of surfactants, the smaller the surface tension γ . If the surface concentration is not uniformly distributed, the gradients of surface tension induce Marangoni forces, which tend to spread the surfactant uniformly. In a vertical soap film, the surfactant concentration is larger at the bottom than at the top of the film: a vertical gradient of surface tension opposes the hydrostatic pressure exerted by the inner fluid:

$$2 \frac{d\gamma}{dy} = \rho g e(y) \quad (6)$$

where y is the vertical coordinate, ρ the density of the liquid and g the gravity acceleration. The prefactor 2 is due to the presence of two interfaces on the soap film. In the case of an insoluble surfactant, the equilibrium profile of the soap film can be predicted [10,25]. However, this prediction is not valid in the case of a soluble surfactant, which corresponds to the majority of the experiments, since the use of soluble surfactants at high concentrations (i.e. larger than the critical micellar concentration) considerably increases the soap film stability [26].

Considering the 2D system formed by the surfactant molecules in interaction within one interface, the Marangoni force can be seen as an elastic restoring force, which counterbalances the 2D compression (or dilatation) of the surfactant molecules. Hence, the surfactant monolayer is actually provided with 2D visco-elastic properties. The surface elastic modulus of the soap film is defined as:

$$E = 2 \frac{d\gamma}{d(\ln S)} = 2S \frac{d\gamma}{dS} \quad (7)$$

where S is the surface of the film. Since the fluid is incompressible, the volume $V = S \times e$ is a constant and this definition is equivalent to

$$E = -2e \frac{d\gamma}{de}. \quad (8)$$

Using Eqs. (6) and (8), the surface elasticity can then be estimated from the soap film profile [10]:

$$E = -\rho g e^2 \frac{dy}{de}. \quad (9)$$

In our experimental conditions, $e \sim 1\mu\text{m}$ and $dy/de \sim -1,5.10^4$ (estimated for example on Fig.5), which leads to $E \sim 0.15 \text{ mN.m}^{-1}$.

3.3.3 Drainage

On a timescale longer than a few seconds, the coloured fringes slowly fall down in time, indicating that the thickness of the soap film decreases. Indeed, the liquid flows down because of its own weight. The interfaces covered with surfactant

molecules are provided not only with 2D elastic properties but also with 2D viscous properties, hence the motion of the liquid inside the film is slowed down by the viscous friction against the interfaces. The velocity profile of the liquid between the interfaces is a Poiseuille profile with a non-zero velocity at the interfaces which are also set into motion (see [25,27] for details). The drainage stops when the soap film has reached its equilibrium thickness as described in paragraph 3.3.1.

4 Coupling sound and vision: “Seeing” the sound on a soap film

In this section, all the elements that have been separately analysed in the previous section are coupled, to describe the Sound and Vision experiment. Depending on the acoustic excitation, different phenomena appear. Capillary waves can be observed on the soap film even at small forcing amplitude. At larger amplitude the thickness profile is perturbed by the vibration according to a process called self-adaptation. When increasing the forcing amplitude, further non-linear effects appear. Amongst them, we describe the apparition of counter-rotative vortices.

4.1 Capillary waves

Under acoustic forcing, the vibration of the air in the tube forces the soap film to move transversally: a transverse vibration wave propagates along the liquid membrane. The wave is reflected at the boundaries of the film and at its center. Due to the axial symmetry of the problem, this leads to the apparition of a circular standing wave on the soap film. This wave is characterized by the displacement $z(r, t) = A_0 J_0(2\pi r/\lambda_f) \cos(2\pi f t)$, where $z(r, t)$ is the transverse displacement from the equilibrium position at time t and distance r from the center of the film, A_0 is the amplitude at the center, λ_f is the wavelength and J_0 the Bessel function of the first kind and zero order, whose profile is sketched in Fig. 7(a). When the soap film is illuminated and observed within a direction close to the normal incidence, the curved interface of the oscillating film acts as a curved mirror that focalizes the light reflected around the antinodes (caustics). This explains the appearance of bright rings on the soap film as shown in Fig. 7(b), whose number increases when the acoustic frequency increases.⁴ This ring pattern allows the measurement, using image analysis, of the wavelength λ_f . The variation of λ_f with the acoustic frequency can then be compared with previous works ([14, 18] and references therein) that predict the following dispersion relation between the wavelength and the frequency, for a horizontal infinite soap film, and in the linear limit with $A_0, e \ll \lambda_f$:

$$\lambda_f f = \sqrt{\frac{2\gamma}{\rho e + \rho_a \lambda_f / \pi}} \quad (10)$$

⁴Note that a parallel illuminating beam light would generate a more contrasted ring pattern [28].

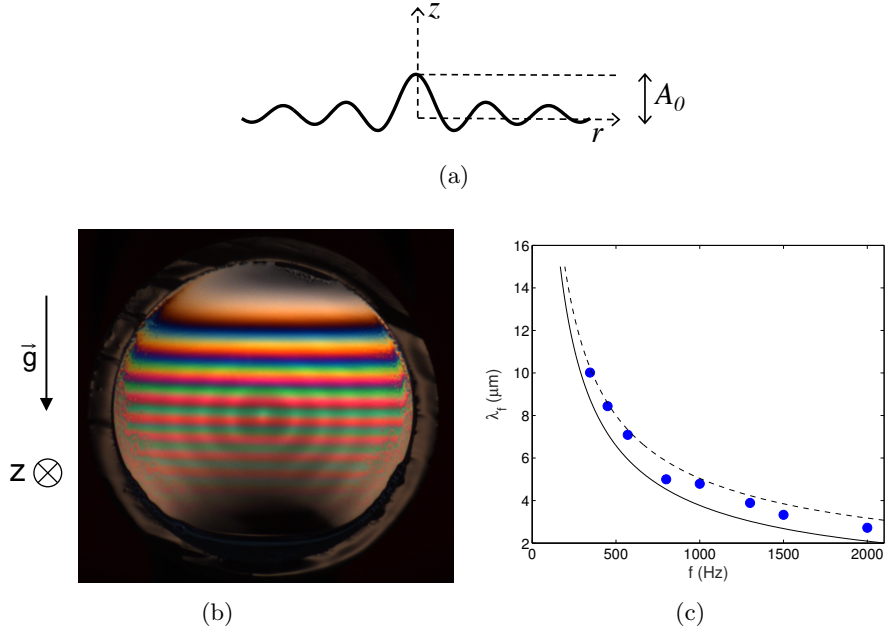


Figure 7: (a) Schematized side view of a vibrating film following a Bessel profile: $z(r) = A_0 J_0(2\pi r / \lambda_f)$. (b) Photograph (front view) of a vibrating soap film, presenting a standing capillary wave, visible *via* the bright concentric rings (colours online). The acoustic frequency is 860 Hz. (c) Wavelength λ_f of the capillary waves as a function of the frequency f . The symbols represent the experimental points, and the black curves the theoretical dispersion relation given by Eq. (10), for two values of the thickness e (full line: $e = 2 \mu\text{m}$, dashed line $e = 0 \mu\text{m}$).

where ρ and ρ_a are the densities of the soap solution and of the air. The wave propagation is characterized by the interplay between the surface tension γ as the restoring force, and the inertia of the system. Note that the inertia of the air above and below the film on a typical distance λ_f has to be taken into account, since $\rho_a \lambda_f$ and ρe are of the same order of magnitude.

Considering that in our experiments the thickness of the soap film is not homogeneous because of the gravitational drainage, we find a good agreement between the theoretical predictions and our measurements of λ_f , as shown in Fig. 7(c).

4.2 Self-adaptation of the thickness

When increasing the amplitude of the acoustic excitation, the interference fringes are not horizontal anymore as shown in Fig. 8(a): they undulate and exhibit peaks

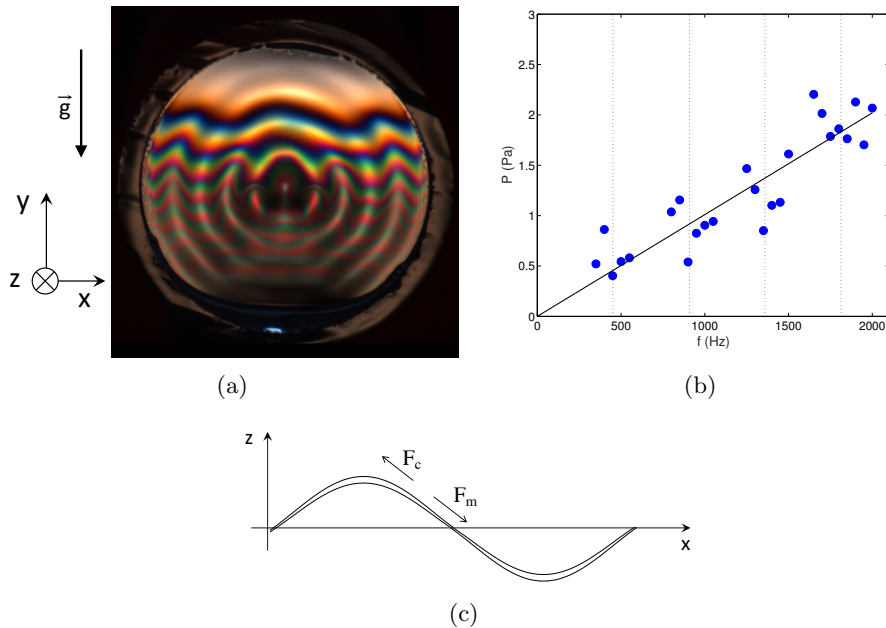


Figure 8: (a) Photograph of a soap film acoustically excited, showing self-adaptation (colours online). (b) Minimum amplitude of the pressure for the apparition of self-adaptation, as a function of the applied frequency. The measurements have been made around the resonances frequencies of the tube (indicated by the vertical dashed lines), where high enough forcing amplitudes can be obtained. The black curve is a linear fit of the experimental points: $P = 1 \times 10^{-3} \times f$. Each measurement has been performed on a different soap film, by increasing gradually the amplitude of a monochromatic forcing until self-adaptation appears. (c) Sketch of a vibrating soap film exhibiting self-adaptation. The centrifugal force F_c creates a tangential flow inside the film towards the antinodes, whereas the Marangoni force F_m tends to homogenize the thickness of the film.

around the antinodes of the transverse vibration. This means that a liquid flow has occurred in the plane of the film, leading to a spatial modulation of the soap film thickness: the film is thinner around the vibration nodes and thicker around the antinodes. This phenomenon, already observed in a previous work (see [17]), is referred to as *self-adaptation*. We have observed that the self-adaptation appears above a threshold value of the amplitude of the acoustic wave, which depends linearly on the frequency, as presented on Fig. 8(b).

We develop here a simple argument to explain this effect, based on the modeling

performed by Boudaoud *et.al.* [17]. We consider a two-dimensional problem in the (x, z) plane, where x is tangent to the soap film at rest and z is the normal axis (Fig. 8). z is also the transverse displacement of the film, and we call u the tangential liquid velocity inside the film (assumed to be small compared to the transverse velocity). Moreover, the gravity and the inertia of the air are neglected here (they play no role in this mechanism). The equations of motion for the liquid, projected respectively along the transverse axis z and in the plane of the soap film, are:

$$\rho e \frac{\partial^2 z}{\partial t^2} = 2\gamma \frac{\partial^2 z}{\partial x^2} + P \cos(2\pi ft) \quad (11)$$

$$\rho e \frac{\partial u}{\partial t} = F_m + F_c. \quad (12)$$

In Eq. (11), the first term of the right-hand side describes the interfacial force per unit area that tends to minimize the curvature of the soap film, and P is the amplitude of the acoustic pressure in the tube. To describe the dynamics of the tangential velocity u in Eq. (12), two forces are in competition, as sketched in Fig. 8(c). On the one hand, the vertical acceleration of the film has a non-zero component in the plane of the soap film, which leads to the inertial centrifugal force per unit area:

$$F_c = -\rho e \frac{\partial^2 z}{\partial t^2} \frac{\partial z}{\partial x}. \quad (13)$$

Assuming $z = A \cos(qx) \cos(\omega t)$, with $q = 2\pi/\lambda_f$ and $\omega = 2\pi f$, the centrifugal force can be written:

$$F_c = -\rho e q \omega^2 \frac{A^2}{2} \sin(2qx) \cos^2(\omega t). \quad (14)$$

Since the time-average $\langle \cos^2(\omega t) \rangle = 1/2$ over one period, this force does not average to zero. F_c is always directed towards the antinodes: it is thus responsible for the flow of liquid inside the film from the nodes towards the antinodes, leading to the thickening (resp. thinning) of the antinodes (resp. nodes). Hence, a periodic thickness modulation builds up with a spatial period equal to $\lambda_f/2$: $e = e_0 + \delta e \cos(2qx)$. On the other hand, the Marangoni force per unit area:

$$F_m = 2 \frac{\partial \gamma}{\partial x} = -\frac{E}{e} \frac{\partial e}{\partial x} = +E \frac{\delta e}{e} 2q \sin(2qx) \quad (15)$$

tends to homogenize the thickness of the soap film (the elasticity E defined by Eq. (8) is assumed to be constant).

The existence of a stationary regime implies $\langle F_c \rangle = \langle F_m \rangle$, where $\langle F \rangle$ means that the quantity F is time-averaged over a period $1/f$. This leads to $\rho e \omega^2 q A^2/4 \sim (E/e) 2q \delta e$. From Eq. 11 we get $A \sim P/(\rho e \omega^2)$, and we finally obtain:

$$P \sim \omega \sqrt{8\rho E \delta e}. \quad (16)$$

Finally, to compare to our experimental measurements, we assume that the self-adaptation becomes visible when the thickness variation δe is of the order of the

one corresponding to one fourth of order of interference (see Fig. 8(a)): $\delta e_{min} \sim 50$ nm. This leads to a threshold amplitude for the acoustic pressure:

$$P > 2\pi f \sqrt{8\rho E \delta e_{min}} \sim 1.4 \times 10^{-3} \text{ Pa.s} \times f \quad (17)$$

with $E = 0.15$ mN/m (see section 3.3.2) and $\rho = 10^3$ kg/m³. This order of magnitude is in good agreement with our experimental results presented in Fig. 8(b).

4.3 Vortices

When increasing further the amplitude of the acoustic pressure above self-adaptation threshold, the system becomes unstable and vortices appear in the soap film. A very rich and complex phenomenology appears. We describe on the photographs of Fig. 9 a scenario for the apparition and evolution of such vortices, under a continuous monochromatic acoustic forcing suddenly started at $t = 0$. Within a fraction of second, liquid is observed to accumulate around the vibration antinodes and self-adaptation appears as shown in Fig. 9(a). Then, recirculation of liquid is observed at $t \sim 1$ s and vortices form in the region of thin film around the nodes and in the upper region of thin film of the soap film as shown in Fig. 9(b). The vortices always appear by pair of opposite circulation. The vortices then grow and accelerate (Fig. 9(c)), sometimes merge in pairs, and finally disappear spontaneously after a few seconds (Fig. 9(d)). After the vortices have disappeared, self-adaptation is still present, and the gradient of thickness is much smaller than in the initial condition of Fig. 9(a).

The building up of vortices is certainly the key ingredient for the beauty of the experiments, since the liquid is advected whereas the thickness gradients do not disappear: colours are therefore advected as well, producing wonderful dynamical patterns. However, the appearance of vortices invokes complex mechanisms and no simple overall picture exists yet in the literature. In the case of a horizontal soap film vibrated transversally, two main mechanisms have been identified.

Firstly, at large enough acoustic pressure, strong nonlinear effects due to the inertia of the liquid become important, besides Marangoni and centrifugal forces. This non-oscillatory volume forcing, originating inside the liquid, strongly depends on the thickness gradient [16]. In the case of our experiments, the existence of a large thickness gradient due to the gravitational drainage of the film could enhance this non-oscillatory volume forcing of the vortices. Moreover the spontaneous disappearance of the vortices after a while is concomitant with a decrease in the thickness gradient, which comforts this interpretation.

Secondly, another source of non-linearity is due to the motion of the air above and below the film. For high amplitudes in film vibration, inertial effects in the air results in steady recirculations with several cellular motions [10,15,16] (and see [29] about this effect called *acoustic streaming*). This effect is due to the non-linearities of the stress appearing in the Stokes layers and may result in a non negligible tangential flow of the liquid (surface forcing). This flow could lead to a gradient of thickness, and then a gradient of surface tension, reinforcing the competition between opposite forces at the origin of the vortices.

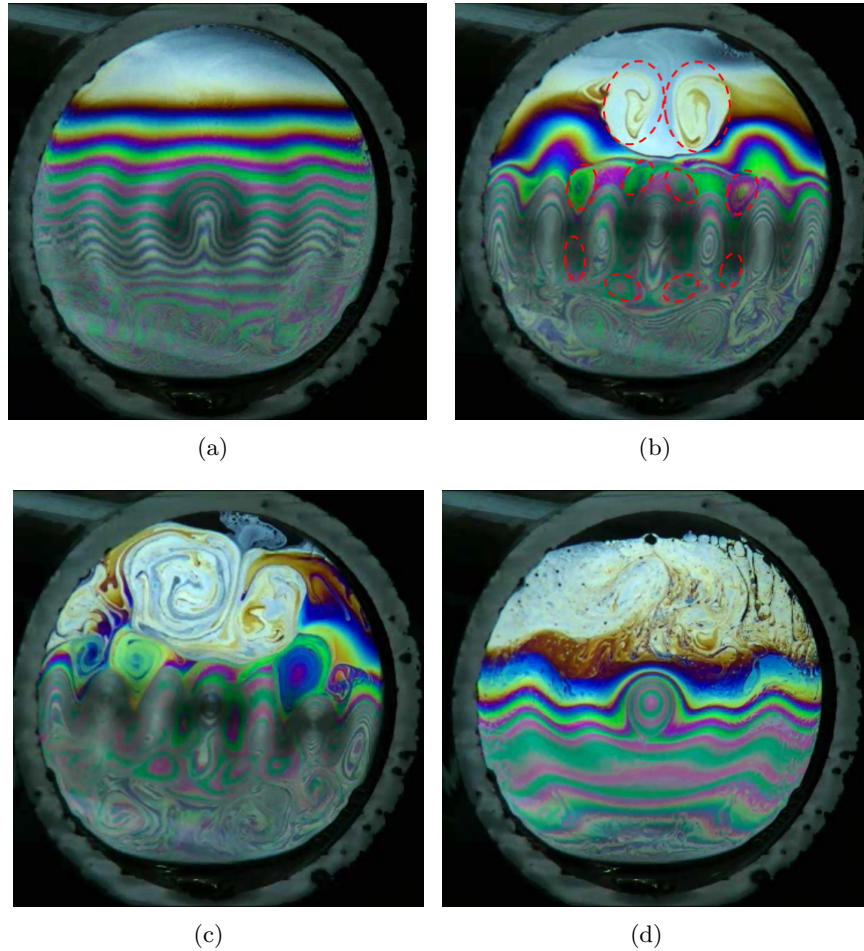


Figure 9: Time sequence of the birth and death of vortices (colours online). A monochromatic acoustic wave ($f = 450$ Hz, $P = 0.5$ Pa) is set at $t = 0$ s. (a) $t = 0.1$ s: just after the beginning of the acoustic emission, only self-adaptation is visible. (b) $t = 7$ s: the vortices, that appeared after $t = 1$ s, are growing. For clarity they have been highlighted on the picture by dashed red ellipses: the vortices are organised around the antinodes which are made visible by the tight interference fringes. (c) $t = 12$ s: the vortices grow and accelerate gradually. (d) $t = 17$ s: the vortices disappear although the acoustic excitation is still present.

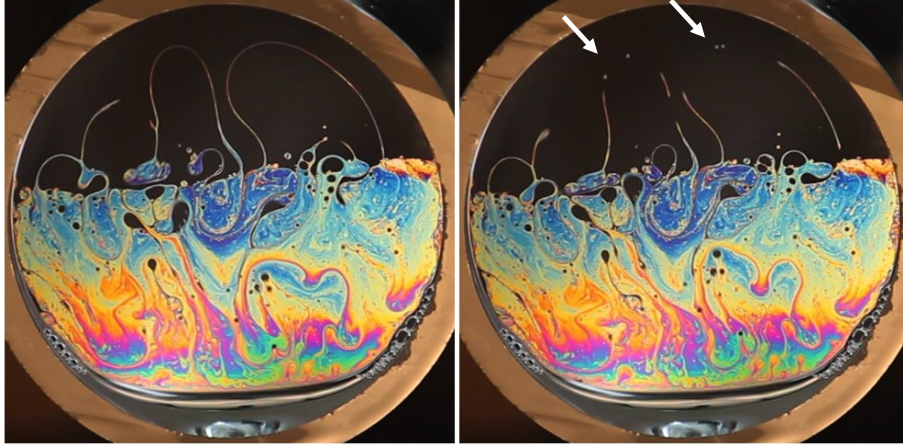


Figure 10: “Bubbles” of black film trapped inside the iridescent film, and drops and filaments of iridescent film inside the black film region (colours online). The filaments have been formed during the ascending motion of liquid advected by a vortex before the image is taken. The two images are separated by 0.3 seconds. The rising up of the 2D bubbles is visible, as well as the destabilization of the 2D coloured filaments into 2D droplets, which has been pointed by white arrows. Piece of music: *Lucilla*, from the album ‘Aeroplanando’, by Choro de Rua (2013).

4.4 Two-dimensional rising bubbles and falling drops

The vortices drive zones of inhomogeneous thicknesses, which travel in the soap film and do not merge with the surrounding. The result is spectacular when a significant initial fraction of the soap film surface is a black film, as shown on Fig. 1 and 10. Two-dimensional (2D) “bubbles” formed of black film can be trapped inside the iridescent film, and similarly 2D drops of coloured film may be advected in the black film region during the acoustic forcing. These 2D domains behave as if the black film region and the coloured film region were two immiscible phases, separated by a 1D interface. Fig. 10 shows that the drops and bubbles are circular, suggesting that the interface tends to be minimal. Moreover coloured filaments fragment into several drops, driven by the interface minimisation. The one-dimensional interface between areas of black film and of iridescent film thus behaves like the interface between immiscible phases in 3D system driven by the surface tension: by analogy, a line tension can then be used to describe the line energy of the interface between those 2D domains.

When the acoustic forcing is removed, the bubbles rise up and burst at the 2D surface of the coloured film, mimicking the buoyancy motion of air bubbles in a liquid pool. Why do bubbles rise? As described by Eq. (6) (sec. 3.3.2), the

hydrostatic pressure inside the vertical soap film at rest equilibrates the gradient of surface tension (the Marangoni force), both depending on the local thickness of the soap film. When a region of black film is trapped inside an iridescent area of much larger thickness, the local Marangoni force is larger than its weight and the “bubble”, experiencing a net upwards force, is driven up until it reaches a region matching its thickness. Everything happens as if the black film drops, even though they have the same density as the surrounding, were lighter and thus were submitted to an Archimedes buoyancy force. Similarly, drops of large thickness which have been dragged into the black film fall down in the iridescent pool until the Marangoni force is large enough to equilibrate its weight.

4.5 Swelling the soap film

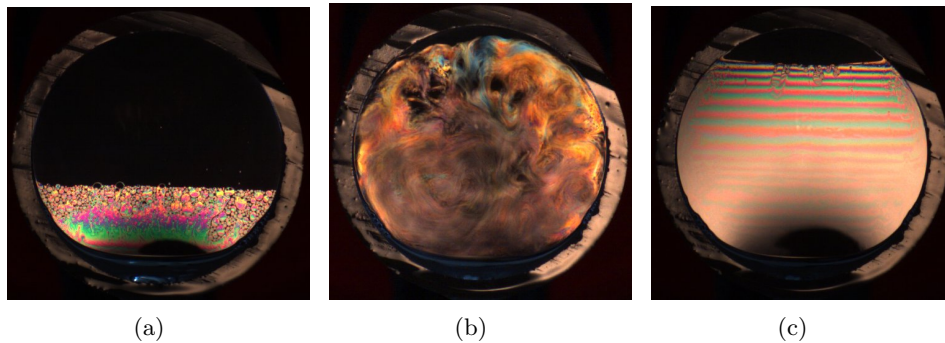


Figure 11: Acoustic swelling of a soap film. (a) In the initial state, a large surface fraction of the vertical soap film is black. (b) The amplitude of the acoustic excitation is suddenly increased: large recirculations of liquid within the whole film is observed. (c) The acoustic forcing is removed: a large surface fraction of the film is now filled with coloured fringes. The time elapsed between each image is ~ 1 s (colours online).

Increasing even further the amplitude of the acoustic forcing may conduct to swell the soap film previously drained, as illustrated in Fig. 11. Due to drainage, a large surface fraction of the film is initially black (Fig. 11(a)). The acoustic forcing is then set at a high amplitude and a large recirculation of liquid happens as shown in Fig. 11(b). At the internal bottom of the tube, liquid pool is always present, coming from liquid dragged during the soap film formation when the end of the tube is dipped in the soap solution, or from the liquid which has drained out of the film. The flow in the plane of the film advects liquid from this reservoir, which swells the soap film. When the acoustic forcing is removed, coloured fringes appear on a large surface fraction of the film in Fig. 11(c), showing that the film is thicker than initially. This swelling of a vertical soap film using an acoustic wave has to our

knowledge never been previously reported in the literature; we plan to investigate this effect in detail in further studies.

5 Conclusion: the key of an aesthetic experiment

When the acoustic forcing is a music play, all the events described in the previous sections couple, synchronizing the visual events on the music. In this section, we synthesize the phenomena and we show how they combine to produce the impression that we actually “see” what we hear.

5.1 Choice of the tube

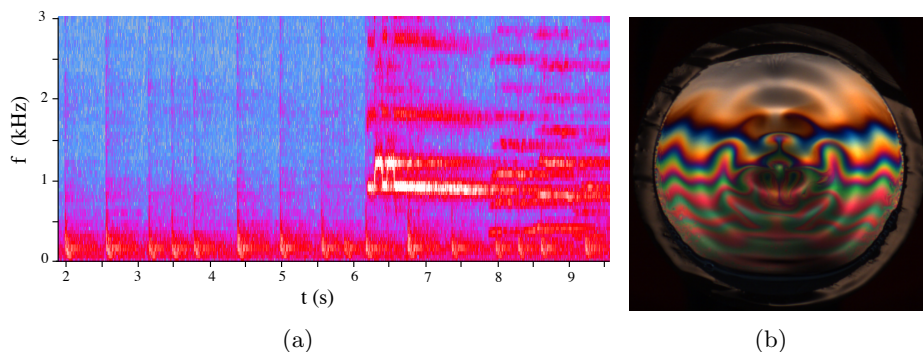


Figure 12: (a) Part of the spectrogram (obtained using the free software Audacity[®]) from *The Good, the Bad and the Ugly main theme*, soundtrack by Ennio Morricone. The frequency content of the music played is displayed versus time. The corresponding amplitude is indicated by a color code (in arbitrary units): a continuously growing amplitude corresponds to a color successively blue, pink, red and then white. Thus, dominant frequencies appear in white, and reflect the melody of the music play (note that the harmonics, which are multiple frequencies of the fundamental frequency, are also present but at a lower amplitude). A short sequence, having a broad spectrum peaked at 200 Hz, appears regularly in time with a periodicity of ~ 1 s: this part is played by drums. Between 6 s and 8 s, the principal frequency varies from 900 Hz to 1250 Hz: this part is played by a flute. The second resonant mode of the tube, of length $L = 35.5$ cm, is at 900 Hz (see Fig. 4). Hence, flow of liquid inside the soap film is observed while the flute is playing, as shown on (b), with a photograph taken at $t = 7$ s (colours online). The extract of the piece of music is visible at the following link: https://youtu.be/YC0cZ_xNf-Y.

The key of the synchronization between music and visualisation resides in the fact that only some frequencies are amplified: the acoustic resonant frequencies of the tube. Phenomena such as self-adaptation, vortices and two-dimensional bubble ejection are more easily obtained at frequencies close to the resonances of the tube, given by equation (3), which depend on the length and on the diameter of the tube. The frequencies of the piece of music can be analyzed using a spectrogram, that represents the frequencies over time, as shown in Fig. 12: a colour code displays the amplitude of the frequencies. The length and diameter of the tube can thus be adapted for the resonant frequencies of the tube to coincide with the dominant frequencies of the music play, which have the highest amplitude. The tube resonant frequencies can also be adapted to the tessitura of the music instrument present in the music play. For example, the fundamental frequency of the tube used in our experiments is around 450 Hz (see Fig.4), which corresponds to the frequency range covered by the flute, or the soprano voice. As for percussion instruments (drums, piano etc.), their broad acoustic frequency range makes them adapted to excite the resonant frequency of any tube. Hence the acoustically forced patterns on the soap film at the end of the tube synchronize on the rhythm given by the percussions.

5.2 The interplay of the characteristic time scales

The generation of vortices is certainly the phenomenon by which liquid is advected in the soap film, producing spectacular effects. In section 4.3, the scenario illustrated on Fig. 9 is obtained for a continuous monochromatic acoustic excitation, of constant amplitude, emitted during more than 20s. In the case of a piece of music, the situation is however different. The amplitude is not constant, and both the frequency and the amplitude can vary quickly in time. Vortices can grow and accelerate as previously discussed if the corresponding frequency is played at a large enough amplitude within a few seconds. The photograph of Fig. 13 is a representative example of counter-rotative pairs of vortices observed using a music play as an acoustic forcing. However the characteristic time for their spontaneous disappearance described in Fig. 9 is never reached. With a piece of music vortices disappear rather due to a change of frequency and/or amplitude.

More generally, the observed dynamical patterns involve many characteristic times: one characteristic time for the gravity-induced drainage of liquid in the film (~ 10 s), another for the self-adaptation phenomena (~ 0.1 s), for the development of vortices (~ 1 s), and for their disappearance under forcing (~ 10 s), which reveal the richness of the physics behind those dynamical patterns. Moreover, some characteristic times are also associated to the advection of iridescent domains within the black film. All those characteristic times are involved in the dynamical response of the soap film to the acoustic forcing produced by a music play: they play a major role in the aesthetics of the experiment.

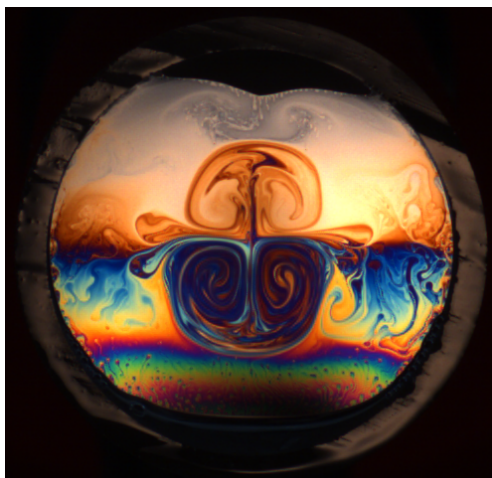


Figure 13: A representative example of counter-rotative pairs of vortices obtained with a piece of music, here *The Good, the Bad and the Ugly* main theme soundtrack by Ennio Morricone (colours onlie).

5.3 Increasing the life-time of the soap film

Due to the drainage, the soap film gets thinner over time, and thus more fragile, *i.e.* more likely to burst. To avoid soap film bursting over several minutes, the film can be swollen by increasing the amplitude of the acoustic forcing, as shown in Fig. 11. This mechanism brings furthermore iridescent soap film in the field of view, and new coloured patterns can be formed. However, one must be careful in increasing the forcing amplitude, since a very large amplitude could lead to the soap film bursting [30].

5.4 To conclude

We emphasize on the fact that, even if each phenomenon can be described separately, they generally occur simultaneously. In Fig. 14 for instance, we can see the concentric bright rings of capillary waves, the deformation of the coloured fringes due to self-adaptation, and also the beginning of vortices at the centre of the film.

To conclude, we have shown the rich and complex dynamics of a soap film in response to a non-continuous sound wave. These physical phenomena involved tackle with acoustics, optics and hydrodynamics. Hence, this experiment is a good candidate for teaching physics in a classroom or for science popularization. Furthermore, the spectacular effect produced by the synchronization of the video and the music makes of this experiment an interesting tool for art and science projects. Finally, this work has also opened a still unexplored research trail based on the acoustic swelling of the soap film.

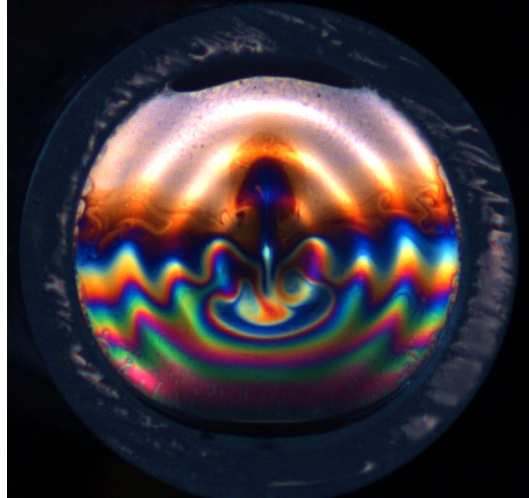


Figure 14: Photograph of a soap film presenting at the same time: capillary waves, self-adaptation and the beginning of vortices. Piece of music: *The lonely shepherd*, from the album “Kill Bill Vol. 1 Original Soundtrack”, by Gheorghe Zamfir (colours online).

Acknowledgements

We warmly thank our colleagues F. Graner, L. Rose, and V. Leroy for the fruitful and enthusiastic discussions. This work was supported by the French Agence Nationale de la Recherche (ANR) through the project SAMOUSSE (ANR-11-BS09-001).

References

- [1] Aristotle, *Complete work of Aristotle, Volume 1: The revised Oxford translation (chapter Sense and Sensibilia)* (Princeton University Press, 1984).
- [2] Newton I., *Opticks, or a Treatise of the reflexions, refractions, inflexions and colours of light* (London, 1704).
- [3] Rimington A. W., *Colour-Music: The art of moving colour* (Hutchinson, 1912).
- [4] The National Gallery (July 2015). *Soundscapes*, Retrieved 28 Nov. 2016 from <https://www.nationalgallery.org.uk/whats-on/soundscapes>.
- [5] Stanford N. (Nov. 2014) *CYMATICS: Science Vs. Music*, Retrieved 4 Jan. 2017 from <https://vimeo.com/111593305>.

- [6] Boys, C. V., *Soap Bubbles and the Forces which Mould Them* (SPCK, London 1890); enlarged edition *Soap Bubbles, their Colours and the Forces which Mould Them*, Dover Publications, New York, 1959.
- [7] Rämme, G., *Soap Bubbles in Art and Education* (Willie Yong, Singapore, 1998) and *textitExperiments with Soap Bubbles and Soap Films* (C, Uppsala, Sweden, 2006).
- [8] D. R. Lovett, *Demonstrating Science With Soap Films* (Institute of Physics Publishing, Bristol and Philadelphia, 1994).
- [9] Isenberg, C. *The Science of Soap Films and Soap Bubbles* (Clevedon, Avon, England: Tieto, 1987; reprinted 1992 New York, Dover).
- [10] Couder Y., Chomaz J.-M. and Rabaud M., *Phys.D*, 1989, **37**, 384.
- [11] Seychelles F., Amarouchene Y., Bessafi M., and Kellay H., *Phys. Rev. Lett.*, 2008, **100**, 144501.
- [12] Tylor E. B., *Nature*, 1877, **16**, 12.
- [13] Taylor S., *Proc. R. Soc.*, 1878, **27**, 71.
- [14] Joosten J.G.H., *J. Chem. Phys.*, 1984, **80**, 2383.
- [15] Afenchenko V.O., Ezersky A.B., Kiyashko S.V., Rabinovich M.I. and Weidman P.D., *Phys.Fluids*, 1998, **10**, 390.
- [16] Vega J. M., Higuera F. J. and Weidman P. D., *J. Fluid Mech.*, 1998, **372**, 213-230.
- [17] Boudaoud A., Couder Y. and Ben Amar M., *Phys.Rev.Lett.*, 1999, **82**, 3847.
- [18] Kosgodagan Acharige S., Elias F. and Derec C., *Soft Matter*, 2014, **10**, 8341.
- [19] Elias F., Hutzler S., Ferreira M. S., *Eur. J. Phys.*, 2007, **28**, 755.
- [20] Rossing T. D., *Handbook of Acoustics* (Springer, 2007).
- [21] Ogawa N. and Kaneko F., *Eur.J.Ph.*, 2013, **34**(5), 1159-1165.
- [22] Delly, J.G. (2003): The Michel-Lévy interference color chart microscopy's magical color key: <https://www.mccrone.com/mm/the-michel-levy-interference-color-chart-microscopys-magical-color-key/>
- [23] Hulbers P. D. T. and Shah D. O., *Langmuir*, 1997, **13**, 5995.
- [24] Cantat I., Cohen-Addad S., Elias F., Graner F., Hohler R., Pitois O., Rouyer F. and Saint-Jalmes A., *Les mousses, Structure et Dynamique* (Belin, Paris, 2010). English translation: *Foams: Structure and Dynamics*, edited by S. J. Cox (Oxford University Press, 2013).
- [25] Schwartz L. W. and Roy R. V., *J. of Colloid ans Interface Science*, 1999, **218**, 309.

- [26] Champougny L., Roché M., Drenckhan W. and Rio E., *Soft Matter*, 2016, **12**, 5276.
- [27] Elias F., Bacri J.-C., Flament C., Janiaud E., Talbot D., Drenckhan W., Hutzler S. and Weaire D., *Colloids and Surfaces A*, 2005, **263**, 65.
- [28] Elias F., Kosgodagan Acharige S., Rose L., Gay C., Leroy V. and Derec C., *Colloids and Surfaces A*, 2017, under revision.
- [29] Nyborg W.L., *J. of Acoust. Soc. Amer*, 1958, **30**, 329.
Lighthill J., *J. of Sound and Vibr.*, 1978, **61**, 418.
- [30] Drenckhan W., Dollet B., Hutzler S. and Elias F., *Phil. Mag. Lett.*, 2008, **88**, 1669.